Int J CARS (2009) 4:37–44
DOI 10.1007/s11548-008-0265-y

ORIGINAL ARTICLE

Myocardium tracking via matching distributions

Ismail Ben Ayed · Shuo Li · Ian Ross · Ali Islam

Received: 10 January 2008 / Accepted: 14 September 2008 / Published online: 28 October 2008

Abstract
Objective The goal of this study is to investigate automatic myocardium tracking in cardiac Magnetic Resonance (MR) sequences using global *distribution matching* via level-set curve evolution. Rather than relying on the pixelwise information as in existing approaches, distribution matching compares intensity distributions, and consequently, is well-suited to the myocardium tracking problem.
Materials and methods Starting from a manual segmentation of the first frame, two curves are evolved in order to recover the endocardium (inner myocardium boundary) and the epicardium (outer myocardium boundary) in all the frames. For each curve, the evolution equation is sought following the maximization of a functional containing two terms: (1) a *distribution matching* term measuring the similarity between the *non-parametric* intensity distributions sampled from inside and outside the curve to the model distributions of the corresponding regions estimated from the previous frame; (2) a gradient term for smoothing the curve and biasing it toward high gradient of intensity. The Bhattacharyya coefficient is used as a similarity measure between distributions. The functional maximization is obtained by the Euler–Lagrange ascent equation of curve evolution, and efficiently implemented via level-set. The performance of the proposed distribution matching was quantitatively evaluated by comparisons with independent manual segmentations approved by an experienced cardiologist. The method was applied to ten 2D mid-cavity MR sequences corresponding to ten different subjects.
Results Although neither shape prior knowledge nor curve coupling were used, quantitative evaluation demonstrated that the results were consistent with manual segmentations. The proposed method compares well with existing methods. The algorithm also yields a satisfying reproducibility.
Conclusion Distribution matching leads to a myocardium tracking which is more flexible and applicable than existing methods because the algorithm uses only the current data, i.e., does not require a training, and consequently, the solution is not bounded to some shape/intensity prior information learned from of a finite training set.

Keywords Myocardium tracking · Magnetic Resonance (MR) · Cardiac imaging · Matching distributions · Bhattacharyya measure · Level-sets

I. Ben Ayed (✉) · S. Li
General Electric Canada (GE Healthcare), London, ON, Canada
e-mail: ismail.benayed@ge.com

I. Ross
London Health Sciences Centre, London, ON, Canada

A. Islam
St. Joseph's Healthcare, London, ON, Canada

Introduction

Tracking the myocardium in Magnetic Resonance (MR) cardiac sequences is of capital importance in diagnosing cardiovascular diseases. The standardized myocardial segmentation [1], which suggests using three circular basal, mid-cavity, and apical 2D slices to generate 17 standardized segments of the myocardium and the left ventricle, is commonly used for regional analysis of the LV function. This standardization maintains consistency with anatomic/autopsy data, optimizes and facilitates accurate intra and cross modality comparisons for research and clinical applications, and allows precise localization using anatomic landmarks [1]. 2D segmentation of the myocardium allows to assess the regional wall motion abnormalities over the 17 standardized 2D segments. This task plays an essential

role in designing pattern recognition systems that aid in the diagnosis of cardiovascular diseases related to localized regions with movement abnormalities. Manual tracing is time-consuming and prone to high variability between human observers. Therefore, an automatic 2D tracking of the myocardium is desired. The latter consists of automatically partitioning a current frame into three regions: the heart chamber, the myocardium, and the background. Although an important research effort has been devoted to this task [2–14], myocardium tracking is still acknowledged as a difficult problem. Such difficulty is due to several reasons [8,12]: (a) the variability in shape/intensity is high from one subject to another; (b) the papillary muscles inside the chamber have an intensity distribution similar to the myocardium distribution; (c) the intensity characteristics of the left ventricle chamber are similar to those of the right ventricle; (d) the contrast is very low, i.e., there is no edge between the epicardium and some cardiac entities.

As discussed by Freedman et al. in [15], most of medical image segmentation techniques compute a pixelwise correspondence between the current image (or frame) and model distributions of shape and intensity. Model distributions are generally learned from a finite training set and embedded in the segmentation process via two standard frameworks: variational level-sets [16] (such as [2–10]) and active appearance/shape models [17] (such as [11–14]).

The current study is most related to the Left Ventricle (LV) tracking investigations following the region-based level set framework [4–8]. In this connection, existing methods commonly state the problem as the minimization of a functional containing two types of constraints: a shape knowledge constraint and an intensity-driven constraint based on the Maximum Likelihood (ML) principle [16,18–20,26]. The latter maximizes the conditional probability of pixel intensity given the assumed model distribution within each segmentation region. The local pixelwise information is insufficient and misleading because of the difficulties related to the myocardium tracking problem. Consequently, the use of geometric prior information (such as shape priors) in conjunction with an intensity-driven ML constraint is inevitable to obtain satisfying results [5–7,10]. Moreover, a ML intensity-driven constraint is sensitive to inaccuracies in estimating model distributions [21]. Similar to level-set approaches, active appearance/shape models [11–14] compute a pixelwise correspondence between the image and the models [15].

In the scope of general-purpose image segmentation, recent studies have shown the advantages and effectiveness of using the *distribution matching* principle in the level set framework [22,23]. This principle consists of comparing distributions rather than computing a pixelwise information. As we will see in the experiments ("Results"), distribution matching is well-suited to the difficulties related to myocardium tracking.

In this study, we devise distribution matching to myocardium tracking. Starting from a manual segmentation of the first frame, two curves are evolved in order to recover the endocardium (inner myocardium boundary) and the epicardium (outer myocardium boundary) in all the frames. For each curve, the evolution equation is sought following the maximization of a functional containing two terms: (1) a distribution matching term measuring the similarity between the intensity distributions sampled from inside and outside the curve to the model distributions of the corresponding regions estimated from the previous frame; (2) a gradient term for smoothing the curve and biasing it toward high gradient of intensity. The Bhattacharyya coefficient is used as a similarity measure between distributions. The functional maximization is obtained by the Euler–Lagrange ascent equation of curve evolution, and efficiently implemented via level-set.

The proposed functional leads to a myocardium tracking method which has two important advantages over existing ones. First, the proposed method does not require a training. Geometric prior information, such as shape cues, is not necessary to obtain satisfying results because the distribution matching terms prevent both the papillary muscles from being included into the myocardium and the epicardium boundary from spilling into the background. Second, no assumption is made as to the properties of the parametric distributions of intensity/shape data. Those advantages are important because the solution is not bounded to some shape/intensity properties learned from a finite training set, and consequently, the current method is more flexible and applicable than existing ones.

The remainder of this paper is organized as follows. In the next section we define the proposed tracking functionals and derive the corresponding level set evolution equations. "Results" describes an evaluation by quantitative comparisons with independent manual segmentations as well as with another recent method [2]. It also reports an assessment of the reproducibility of the algorithm using two independent runs with two independent observer initializations. The advantages and limitations of the proposed method are mentioned in "Discussion". The last section contains a conclusion.

Materials and methods

Tracking functionals

Let $I_n : \Omega \subset \mathbb{R}^2 \rightarrow \mathbb{R}^+$ be frame n in a MR cardiac sequence containing N frames ($n \in [1, \ldots, N]$). N is typically equal to 20 or 25. Our objective is to partition Ω into three regions: the chamber C_n, the myocardium M_n, and the background B_n. To this end, we consider two closed planar parametric curves: $\gamma_{\text{in}}(s) : [0, 1] \rightarrow \Omega$, and $\gamma_{\text{out}}(s) : [0, 1] \rightarrow \Omega$. The method consists of evolving γ_{in} and γ_{out}, respectively,

toward the endocardium and the epicardium. For each curve, the evolution equation is sought following the maximization of an original functional based on distribution matching. *The idea is to divide frame I_n into three regions whose intensity distributions most closely match the distributions of the chamber, the myocardium, and the background in the previous frame*.

Consider the following definitions:

- $\mathbf{R}_\gamma$ is the region inside curve γ ($\gamma = \gamma_{\text{in}}, \gamma_{\text{out}}$), and $\mathbf{R}_\gamma^c$ its complement, i.e., the region corresponding to the exterior of γ.
- $P_{\mathbf{R},I}$ is the nonparametric (kernel-based) estimates of the distribution of intensity within region $\mathbf{R}$ in frame I:

$$\forall z \in \mathbb{R}^+,\ P_{\mathbf{R},I}(z) = \frac{\int_{\mathbf{R}} \delta(z - I(x))\mathrm{d}x}{\int_{\mathbf{R}} \mathrm{d}x} \tag{1}$$

- $\mathcal{B}(f, g)$ is the Bhattacharyya coefficient [1] measuring the amount of overlap (similarity) between two statistical samples f and g [21]

$$\mathcal{B}(f, g) = \sum_{z \in \mathbb{R}^+} \sqrt{f(z)g(z)} \tag{2}$$

- $(C_{n-1},\ M_{n-1},\ B_{n-1})$ is the partition of Ω (segmentation) obtained in the previous frame (frame $n-1$), with C_{n-1} the region corresponding to the heart chamber, M_{n-1} the region corresponding to the myocardium, and B_{n-1} the region corresponding to background, i.e., B_{n-1} is the complement of $C_{n-1} \cup M_{n-1}$.

We assume that the segmentation of the first frame (frame 1) is performed manually, i.e., regions C_1, M_1, and B_1 are hand-labeled by the user. For each frame n, $n \in [2, \ldots, N]$, we propose to maximize the following functionals:

$$\begin{aligned}
&\mathcal{F}_{\text{in}}(\gamma_{\text{in}}, I_n) \\
&= \underbrace{\alpha\mathcal{B}(P_{\mathbf{R}_{\gamma_{\text{in}}},I_n}, P_{C_{n-1},I_{n-1}}) + \alpha\mathcal{B}(P_{\mathbf{R}^c_{\gamma_{\text{in}}},I_n}, P_{M_{n-1}\cup B_{n-1},I_{n-1}})}_{\text{Distribution matching terms}} \\
&\quad \underbrace{-\beta \oint_{\gamma_{\text{in}}} g(\|\nabla I_n\|)\mathrm{d}s}_{\text{Gradient term}} \\
&\mathcal{F}_{\text{out}}(\gamma_{\text{out}}, I_n) \\
&= \alpha\mathcal{B}(P_{\mathbf{R}_{\gamma_{\text{out}}},I_n}, P_{C_{n-1}\cup M_{n-1},I_{n-1}}) + \alpha\mathcal{B}(P_{\mathbf{R}^c_{\gamma_{\text{out}}},I_n}, P_{B_{n-1},I_{n-1}}) \\
&\quad -\beta \oint_{\gamma_{\text{out}}} g(\|\nabla I_n\|)\mathrm{d}s
\end{aligned} \tag{3}$$

[1] Note that the value of $\mathcal{B}$ are always in [0, 1], where 0 indicates that there is no overlap, and 1 indicates a perfect match.

with g a monotonically decreasing function: $g(t) = \frac{1}{1+t^2}$, and α, β are positive real constants to balance the contribution of each term.

Curve evolution equations

The curve evolution equations are obtained following the maximization of $\mathcal{F}_{\text{in}}$ with respect to γ_{in}, and $\mathcal{F}_{\text{out}}$ with respect to γ_{out}. To this end, we derive the Euler–Lagrange ascent equations by embedding curve γ, $\gamma = \gamma_{\text{in}}, \gamma_{\text{out}}$, in a one-parameter family of curves: $\gamma(s, t) : [0, 1] \times \mathbf{R}_+ \to \Omega$, and solving the partial differential equation:

$$\begin{aligned}
\frac{\partial\gamma_{\text{in}}(s,t)}{\partial t} &= \frac{\partial\mathcal{F}_{\text{in}}}{\partial\gamma_{\text{in}}} \\
\frac{\partial\gamma_{\text{out}}(s,t)}{\partial t} &= \frac{\partial\mathcal{F}_{\text{out}}}{\partial\gamma_{\text{out}}}
\end{aligned} \tag{4}$$

Partition $(C_n,\ M_n,\ B_n)$ of frame I_n is obtained from γ_{in} and γ_{out} at convergence, i.e., when $t \to \infty$, as follows: $C_n = \mathbf{R}_{\gamma_{\text{in}}}$, $M_n = \mathbf{R}^c_{\gamma_{\text{in}}} \cap \mathbf{R}_{\gamma_{\text{out}}}$, and $B_n = \mathbf{R}^c_{\gamma_{\text{out}}}$.

After some algebraic manipulations, (4) yields the final curve evolution equations:

$$\begin{aligned}
\frac{\partial\gamma_{\text{in}}(s,t)}{\partial t} = \Bigg\{ &\frac{\alpha}{\int_{\mathbf{R}_{\gamma_{\text{in}}}} \mathrm{d}x} \Bigg(\underbrace{\sqrt{\frac{P_{C_{n-1},I_{n-1}}(s)}{P_{\mathbf{R}_{\gamma_{\text{in}}},I_n}(s)}}}_{\text{pixelwise correspondence}} \\
&- \underbrace{\mathcal{B}(P_{\mathbf{R}_{\gamma_{\text{in}}},I_n}, P_{C_{n-1},I_{n-1}})}_{\text{distribution correspondence}} \Bigg) \\
&- \frac{\alpha}{\int_{\mathbf{R}^c_{\gamma_{\text{in}}}} \mathrm{d}x} \Bigg(\sqrt{\frac{P_{M_{n-1}\cup B_{n-1},I_{n-1}}(s)}{P_{\mathbf{R}^c_{\gamma_{\text{in}}},I_n}(s)}} \\
&- \mathcal{B}(P_{\mathbf{R}^c_{\gamma_{\text{in}}},I_n}, P_{M_{n-1}\cup B_{n-1},I_{n-1}}) \Bigg) \\
&- \beta g(\|\nabla I_n\|)\kappa_{\text{in}} + \beta\nabla g.\mathbf{n}_{\text{in}} \Bigg\} \mathbf{n}_{\text{in}}
\end{aligned}$$

$$\begin{aligned}
\frac{\partial\gamma_{\text{out}}(s,t)}{\partial t} = \Bigg\{ &\frac{\alpha}{\int_{\mathbf{R}_{\gamma_{\text{out}}}} \mathrm{d}x} \Bigg(\sqrt{\frac{P_{C_{n-1}\cup M_{n-1},I_{n-1}}(s)}{P_{\mathbf{R}_{\gamma_{\text{out}}},I_n}(s)}} \\
&- \mathcal{B}(P_{\mathbf{R}_{\gamma_{\text{out}}},I_n}, P_{C_{n-1}\cup M_{n-1},I_{n-1}}) \Bigg)
\end{aligned}$$

$$-\frac{\alpha}{\int_{\mathbf{R}^c_{\gamma_{\text{out}}}} \mathrm{d}x}\left(\sqrt{\frac{P_{B_{n-1},I_{n-1}}(s)}{P_{\mathbf{R}_{\gamma^c_{\text{out}}},I_n}(s)}}\right.$$

$$\left.-\mathcal{B}(P_{\mathbf{R}_{\gamma^c_{\text{out}}},I_n},\, P_{B_{n-1},I_{n-1}})\right)$$

$$\left.-\beta g(\|\nabla I_n\|)\kappa_{\text{out}} + \beta\nabla g.\mathbf{n}_{\text{out}}\right\}\mathbf{n}_{\text{out}} \qquad (5)$$

where $\mathbf{n}_{\text{in}}$ and $\mathbf{n}_{\text{out}}$ are the outward unit normals to, respectively, γ_{in} and γ_{out}. κ_{in} and κ_{out} are the mean curvature functions of, respectively, γ_{in} and γ_{out}.

Implementation

Level set evolution equations

We use the level-set formalism [24] to implement the curve evolution equations in (5). We represent curves γ_{in} and γ_{out}, respectively, by two functions $u_{\text{in}} : \Omega \subset \mathbb{R}^2 \to \mathbb{R}$ ($\gamma_{\text{in}} = \{u = 0\}$) and $u_{\text{in}} : \Omega \subset \mathbb{R}^2 \to \mathbb{R}$ ($\gamma_{\text{out}} = \{u_{\text{out}} = 0\}$), with the region inside γ ($\gamma = \gamma_{\text{in}}, \gamma_{\text{out}}$) corresponding to $u < 0$ ($u = u_{\text{in}}, u_{\text{out}}$). The level-set representation has well-known advantages over an explicit discretization of γ using a number of points on the curve [24]. It can be effected by stable numerical schemes [24]. It is also implicit, intrinsic and parameter free. The level-set representation of variational problems has become very popular in medical image analysis for several reasons:

- The obtained algorithms can be extended to higher dimensions in a straightforward manner.
- Geometric characteristics of the curve, such as curvatures and normals, can be easily derived.

One can show that [24] if the curve evolves according to $\frac{\partial\gamma}{\partial t} = V.\,\mathbf{n}$ (refer to Eq. (5)), where $V : \mathbb{R}^2 \to \mathbb{R}$ and $\mathbf{n}$ the outward unit normal to γ, then the level set function evolves according to $\frac{\partial u(x,t)}{\partial t} = V.\,\|\nabla u\|$.

Weighting parameters

The parameters weighting the relative contribution of the distribution matching terms and the boundary terms are fixed for all the experiments: $\alpha = 200$, $\beta = 20$. Note that the set of parameters verifying $\beta = 0.1\alpha$ seems to be an acceptable weighting.

Data

The algorithm was applied to cine-MR short axis images obtained with a 1.5 Tesla scanner. All the images were obtained during a 10–15 s breath-holds with a temporal resolution of 20 or 25 frames. Note that the algorithm is applicable to other types of images because the solution is based only on the intensity of the current data.

Results

We conducted several tests with MR cardiac sequences. In the following, we first describe a quantitative performance evaluation of the method by comparisons with manual segmentations as well as with another level set method [2]. Then, we give a representative sample of the results for visual inspection.

Quantitative performance evaluation The performance of the proposed distribution matching was evaluated by comparisons with independent manual segmentations approved by an experienced cardiologist. The method was applied to ten 2D mid-cavity MR sequences corresponding to ten different subjects, i.e., 190 frames were automatically segmented. *The weighting parameters were unchanged for all the datasets*: $\alpha = 200$, $\beta = 20$. For each frame, curve initializations and model distributions are obtained from the segmentation of the previous frame. The segmentation of the first frame is provided by the user. Two clinically important measures were evaluated: the *endocardial area* (region enclosed by γ_{in}) and the *epicardial area* (region enclosed by γ_{out}). Area measurements are expressed in pixels. We used the *Dice Metric* (*DM*) to measure the *similarity* (*overlap*) between manual and automatic segmentations. Let $\mathbf{A_a}$, $\mathbf{A_m}$ and $\mathbf{A_{am}}$ be the areas of, respectively, the automatically detected region, the corresponding hand-labeled region and the intersection between them. *DM* is given[2] by $\frac{2\mathbf{A_{am}}}{\mathbf{A_a}+\mathbf{A_m}}$ [2]. The distribution matching yielded a *DM* equal to 0.89 ± 0.09 for all the data (*DM* is expressed as mean $\pm$ standard deviation).

The linear regression plots in Fig. 1 assess the differences between $2\mathbf{A_{am}}$ and $\mathbf{A_a} + \mathbf{A_m}$ for the endo- and epicardial areas. The smaller these differences, the higher the similarities between manual and automatic segmentations. The endo- and epicardial regression lines did not differ significantly from the identity line. To bear comparisons with other recent level set approaches to LV tracking, we give in Table 1 the Dice metric reported in [2]. Although the proposed functional does not embed prior knowledge, i.e., does not require a training, the performances compare very well with existing methods.

The Bland-Altman analysis of reproducibility [25] is shown in Fig. 2. Table 2 reports the statistics of the differences in log areas between two independent automatic segmentations. The manual initializations were done separately by two

[2] *DM* is always in [0, 1]. *DM* equal to 1 indicates a perfect match between manual and automatic segmentation.

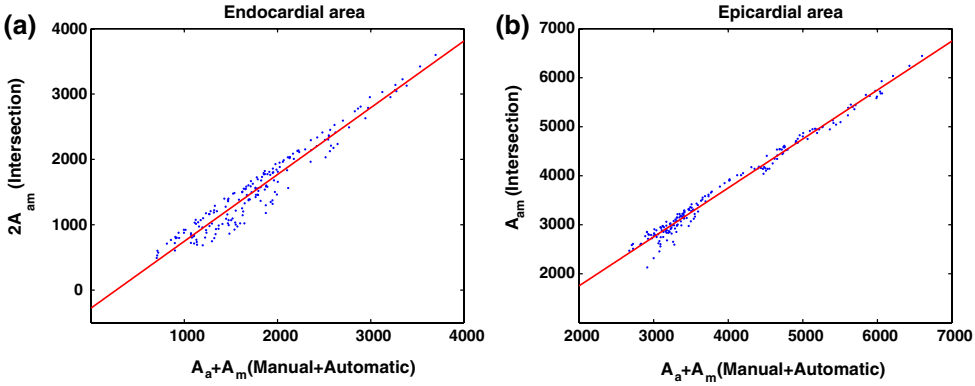

Fig. 1 Comparisons of manual and automatic segmentations in 190 images from 10 datasets. $2\mathbf{A}_{am}$ versus $\mathbf{A_a} + \mathbf{A_m}$: **a** endocardial area, **b** epicardial area

Table 1 Statistical performance evaluation by comparisons of manual and automatic segmentations using the Dice metric

Dice metric	Mean	Std
This method	0.89	0.09
Method in [2]	0.81	0.16

The higher the Dice metric, the better the segmentation

Table 3 Statistics of the DICE measure of reproducibility between two independent automatic segmentations of 190 images from 10 datasets

Dice metric	Mean	Std
Endocardial area	0.9936	0.0077
Epicardial area	0.9791	0.0090

Table 2 Statistics of the differences in Log areas of two independent automatic segmentations of 190 images from 10 datasets

Difference in Log area	Mean	Std
Endocardial area	6.14 (10^{-4})	1.6 (10^{-2})
Epicardial area	2.4 (10^{-3})	3.2 (10^{-2})

different observers. We also give the statistics of the DICE measure of reproducibility between two independent automatic segmentations in Table 3. This demonstrates an acceptable coherence between two independent segmentations.

Visual inspection Figure 3 depicts a representative sample of the tracking results with six typical MR sequences ($s1$–$s6$). $sxfy$ depicts the tracking result obtained for frame y in sequence x. The red and green curves represent, respectively, the obtained γ_{in} and γ_{out} at convergence. The results were also approved visually by a radiologist.

The obtained curves divide each frame into three regions (Fig. 3): the heart chamber (region inside the red curve), the myocardium (region between the red and the green curve), and the background (region outside the green curve). The obtained global distribution flows in the evolution equations (refer to Eq. (5)) prevent both the papillary muscles from being included into the myocardium and the epicardium boundary from spilling into the background. Although neither shape training [5,6] nor curve coupling [8] were used, the results demonstrate that the proposed method deals effectively with the difficulties related to the myocardium tracking problem. Particularly, sequence 5 (the fifth row in Fig. 3) is a low-contrast typical example where the endocardium boundary (the red curve) undergoes high variations in shape over the cardiac cycle. In such situations, geometric cues, such as shape priors, may lead to erroneous results. This demonstrates the flexibility of the proposed method which uses only the intensity of the current data.

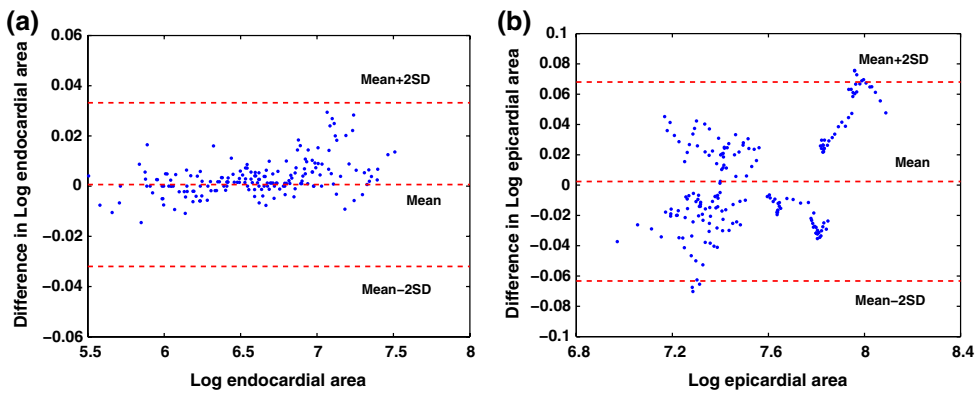

Fig. 2 Bland-Altman plots showing reproducibility of two independent automatic segmentations: **a** differences in Log endocardial areas, **b** differences in Log epicardial areas

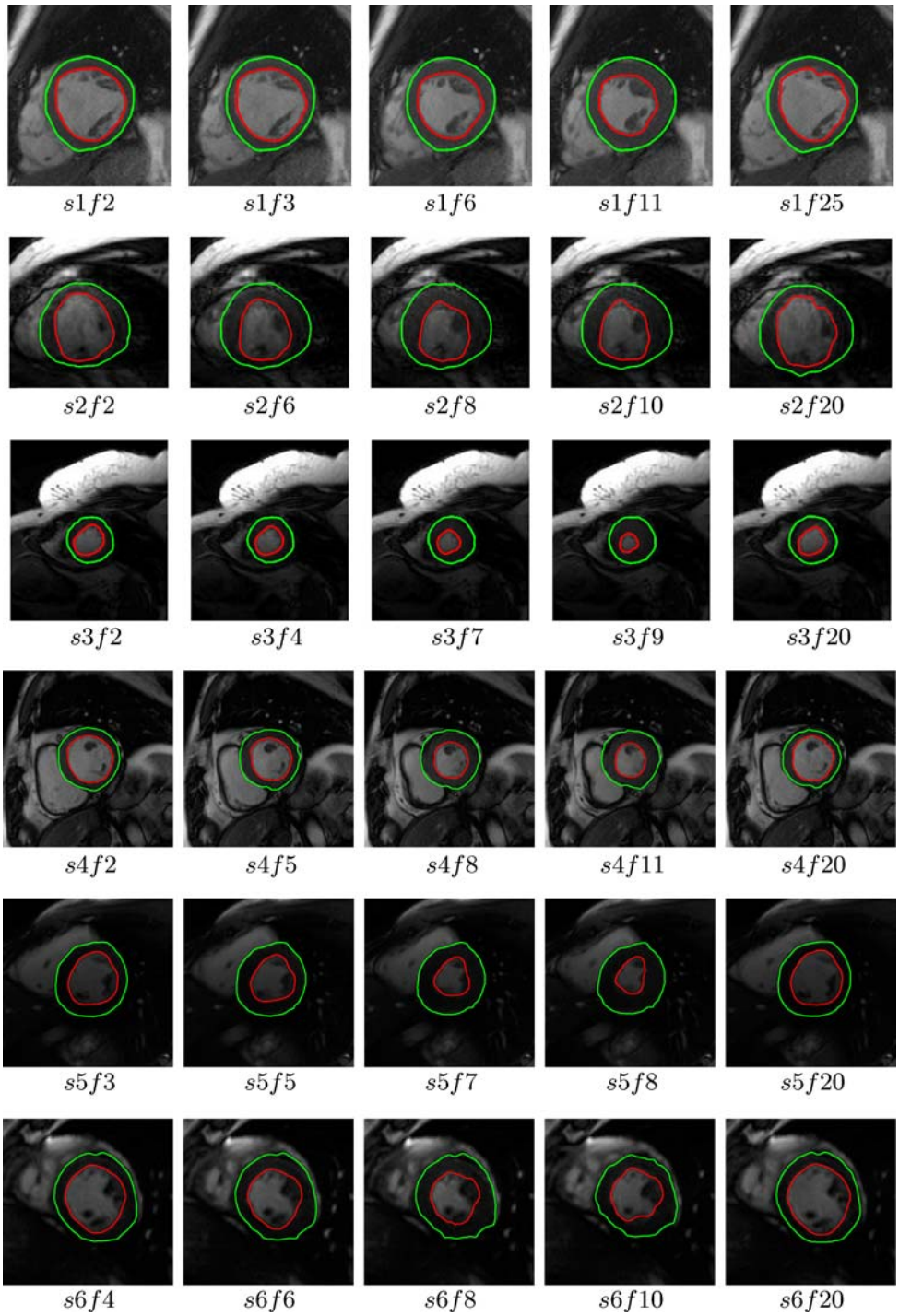

Fig. 3 Tracking results for six MR sequences $s1$–$s6$. Each row depicts the results for one sequence. $sxfy$ depicts the tracking result obtained for frame y in sequence x. The *red* and *green curves* represent, respectively, γ_{in} and γ_{out} at convergence. $\alpha = 200$, $\beta = 20$

Discussion

Although the proposed method is based only on the intensity of the current data, i.e., it does not require a training, the performances compare well with existing methods (refer to Table 1) which, in most cases, use prior knowledge [3–7], such as shape priors, in conjunction with a ML intensity-driven constraint. Different from ML constraints, the proposed distribution matching constraints result in flows (refer to Eq. (5)) which compare not only pixelwise correspondences but also distribution correspondences. The latter prevent both the papillary muscles from being included into

the myocardium and the epicardium boundary from spilling into the background (refer to Fig. 3), thereby relaxing the need of additional geometric priors.

Our method uses the global intensity distribution within the myocardium, and consequently, should be robust to regional intensity variations due to myocardial diseases. We believe that, in the case of regional intensity variations due to myocardial diseases, the distribution matching principle can lead to a competitive performance in comparisons with existing methods because it uses the maximum information available in intensity data.

The proposed method has two important advantages over existing ones. First, geometric prior information is not necessary to obtain satisfying results. This leads to a myocardium tracking which is more flexible and applicable than existing ones because the solution is not bounded to some shape/intensity properties learned from a finite training set. It should be noted that this flexibility comes at the price of a reasonable amount of user interaction–a hand-labeled segmentation of the first frame–because the proposed method requires a reliable estimates of the distributions of regions. A part of our future investigations will focus on automating the initialization. Second, the method computes *non-parametric* distributions, which relaxes assumptions as to the properties of parametric distributions of shape/intensity data. It should be also noted that relaxing such assumptions comes at the price of higher, but reasonable, computational load. With a non-optimized MATLAB implementation running on a 1.66 GHz machine, the algorithm needs approximately 2 min to process a sequence, i.e., 19 frames. A part of our future work will focus on investigating distribution approximations which alleviate the computation of non-parametric distributions. We will also address an extension of the approach to 3D tracking. To extend the approach to 3D + time in a tractable and principled manner, we will use a 3D surface evolution rather than a 2D curve evolution followed by a reconstruction of 2D segmentation results. Note that the level set representation of evolving interfaces, such as 2D curves and 3D surfaces, is parameterization free, and consequently, extends to arbitrary higher dimensions in a straightforward manner. Note that the final evolution equations in (5) apply also for a surface evolution. The only difference is that the domain of the level set function is $\mathbb{R}^3$ rather than $\mathbb{R}^2$. Such implicit representation will implicitly handle the practical difficulties related to reconstructing 2D segmentation results. We are also addressing the problem of automating the LV detection in the first volume because the manual initialization becomes cumbersome in 3D.

The proposed distribution-matching functionals can also be viewed as an alternative to ML constraints in existing systems, i.e., it can be used in conjunction with other geometric cues to improve the performances.

It is worth noting that the method was applied to ten different volunteer with *regular* rhythms because, in general, an irregular heart is a relative counter-indication of cardiac MRI. It affects significantly the visual quality of the data.

Although our method is tested only with mid-cavity MR sequences, we believe that, at the base of the heart, the method can lead to a competitive performance in comparisons with existing methods because it uses the maximum information available in intensity data. Note that due to the complex mixing of the myocardium and connective tissue of the base of the heart, such as the septum, it is difficult to delineate manually or to visualize sufficiently the myocardial wall. Our study follows the recommendations given in the commonly used standardized myocardial segmentation in [1]. This standardization suggests that selecting three representative 2D slices containing the myocardium in all 360 degrees is more appropriate for the LV analysis.

Conclusion

We investigated myocardium tracking using distribution matching. This has led to a method which is more flexible and applicable than existing ones because the solution is not based on a training. Quantitative evaluation by comparisons with independent manual segmentations and with another recent method demonstrated an acceptable performance of the proposed method. The algorithm also yielded a satisfying reproducibility. Future investigations will focus on reducing user interaction as well as computation load.

References

1. Cerqueira MD, Weissman NJ, Dilsizian V, Jacobs AK, Kaul S, Laskey WK, Pennell DJ, Rumberger JA, Ryan T, Verani MS (2002) Standardized myocardial segmentation and nomenclature for tomographic imaging of the heart: a statement for healthcare professionals from cardiac imaging committee of the council on clinical cardiology of the American heart association. Circulation 105:539–542
2. Lynch M, Ghita O, Whelan PF (2008) Segmentation of the left ventricle of the heart in 3-D+t MRI data using an optimized nonrigid temporal model. IEEE Trans Med Imaging 27(2):195–203
3. Lynch M, Ghita O, Whelan PF (2006) Left-ventricle myocardium segmentation using a coupled level-set with a priori knowledge. Comput Med Imaging Graph 30:255–262
4. Jolly M-P (2006) Automatic segmentation of the left ventricle in cardiac MR and CT images. Int J Comput Vision 70(2):151–163
5. Kohlberger T, Cremers D, Rousson M, Ramaraj R, Funka-Lea G (2006) 4D Shape priors for a level set segmentation of the left myocardium in SPECT sequences. MICCAI, pp 92–100
6. Sun W, Çetin M, Chan R, Reddy V, Holmvang G, Chandar V, Willsky A (2005) Segmenting and tracking the left ventricle by learning the dynamics in cardiac images. Inform Process Med Imaging 553–565

7. Paragios N (2003) A level set approach for shape-driven segmentation and tracking of the left ventricle. IEEE Trans Med Imaging 22:773–776
8. Paragios N (2002) A variational approach for the segmentation of the left ventricle in cardiac image analysis. Int J Comput Vision 50(3):345–362
9. Fritscher KD, Pilgram R, Schubert R (2005) Automatic cardiac 4-D segmentation using level sets. In: Frangi A (ed) Proceedings of functional imaging and modelling of the heart. Springer, Heidelberg, pp 113–122
10. Rueckert D, Burger P (1997) Shape-based segmentation and tracking in 4-D cardiac MR images. In: Proceedings of the International Conference on computer vision, virtual reality robotics medicine, CVRMed., Grenoble, pp 43–52
11. Andreopoulos A, Tsotsos JK (2008) Efficient and generalizable statistical models of shape and appearance for analysis of cardiac MRI. Med Image Anal
12. Zambal S, Hladůvka J, Bühler K (2006) Improving segmentation of the left ventricle using a two-component statistical model. MICCAI, pp 151–158
13. Mitchell SC, Lelieveldt BPF, van der Geest RJ, Bosch HG, Reiber JHC, Sonka M (2001) Multistage hybrid active appearance model matching: segmentation of left and right ventricles in cardiac MR images. IEEE Trans Med Imaging 20(5):415–423
14. Stegmann MB, Ólafsdóttir H, Larsson HBW (2005) Unsupervised motion-compensation of multi-slice cardiac perfusion MRI. Med Image Anal 9(4):394–410
15. Freedman D, Radke RJ, Zhang T, Jeong Y, Lovelock DM, Chen GTY (2005) Model-based segmentation of medical imagery by matching distributions. IEEE Trans Med Imaging 24(3):281–292
16. Cremers D, Rousson M, Deriche R (2007) A review of statistical approaches to level set segmentation: integrating color, texture, motion and shape. Int J Comput Vision 62:249–265
17. Cootes T, Edwards G, Taylor C (2001) Active appearance models. IEEE Trans Pattern Anal Mach Intell 23(6):681–685
18. Ben Ayed I, Hennane N, Mitiche A (2006) Unsupervised variational image segmentation/classification using a Weibull observation model. IEEE Trans Image Process 15(11):3431–3439
19. Chan TF, Vese LA (2001) Active contours without edges. IEEE Trans Image Process 10(2):266–277
20. Ben Ayed I, Mitiche A, Belhadj Z (2006) Polarimetric image segmentation via maximum-likelihood approximation and efficient multiphase level-sets. IEEE Trans Pattern Anal Mach Intell 28(9):1493–1500
21. Michailovich OV, Rathi Y, Tannenbaum A (2007) Image segmentation using active contours driven by the Bhattacharyya gradient flow. IEEE Trans Image Process 16(11):2787–2801
22. Zhang T, Freedman D (2005) Improving performance of distribution tracking through background mismatch. IEEE Trans Pattern Anal Mach Intell 27(2):282–287
23. Freedman D, Zhang T (2004) Active contours for tracking distributions. IEEE Trans Image Process 13(4):518–526
24. Sethian J (1999) Level set methods and fast marching methods. Cambridge University Press, London
25. Bland JM, Altman DG (1986) Statiscal methods for assessing agreement between two methods of clinical measurements. Lancet 8476:307–310
26. Ben Ayed I, Mitiche A, Belhadj Z (2005) Multiregion level-set partitioning of synthetic aperture radar images. IEEE Trans Pattern Anal Mach Intell 27(5):793–800